High Temperature Magnetic Ordering in the 4*d* Perovskite $SrTcO_3$

Efrain E. Rodriguez,[1] Frédéric Poineau,[2] Anna Llobet,[3] Brendan J. Kennedy,[4] Maxim Avdeev,[5] Gordon J. Thorogood,[6] Melody L. Carter,[6] Ram Seshadri,[7] David J. Singh,[8] and Anthony K. Cheetham[9]

[1]*NIST Center for Neutron Research, National Institute of Science and Technology, 100 Bureau Drive, Gaithersburg, Maryland 20889, USA*
[2]*Harry Reid Center for Environmental Studies, University of Nevada, Las Vegas, Nevada 89154-4009, USA*
[3]*Manuel Lujan Neutron Scattering Center, Los Alamos National Laboratory, Los Alamos, New Mexico 87545, USA*
[4]*School of Chemistry, University of Sydney, Sydney, Australia*
[5]*Bragg Institute, Australian Nuclear Science and Technology Organisation, Private Mail Bag 1, Menai NSW 2234 Australia*
[6]*IME Australian Nuclear Science and Technology Organisation, Private Mail Bag 1, Menai NSW 2234 Australia*
[7]*Materials Department, Materials Research Laboratory, University of California, Santa Barbara, California 93106, USA*
[8]*Materials Science and Technology Division, Oak Ridge National Lab, Oak Ridge, Tennessee 37831, USA*
[9]*Department of Materials Science and Metallurgy, University of Cambridge, Pembroke Street, Cambridge, CB2 3QZ, United Kingdom*

(Received 18 October 2010; published 7 February 2011)

We present evidence for possibly the highest magnetic ordering temperature in any compound without 3*d* transition elements. Neutron powder diffraction measurements, at both time-of-flight and constant wavelength sources, were performed on two independently prepared $SrTcO_3$ powders. $SrTcO_3$ adopts a distorted perovskite structure with *G*-type antiferromagnetic ordering and has a moment of $1.87(4)\mu_B$ per Tc cation at room temperature with an extraordinarily high Néel point close to 750 °C. Electronic structure calculations reveal extensive mixing between the technetium 4*d* states and oxygen states proximal to the Fermi level. This hybridization leads to a close relationship between magnetic ordering temperature and moment formation in $SrTcO_3$.

DOI: 10.1103/PhysRevLett.106.067201 PACS numbers: 75.50.Ee, 28.20.Cz, 75.47.Lx

The mixed metal oxides of the second transition series exhibit a diverse range of interesting electronic properties. For example, the perovskite Sr_xNbO_3 is a poorly conducting Pauli paramagnet [1], and $SrRuO_3$ a rare example of a metallic ferromagnetic oxide, [2,3]; $SrMoO_3$ shows one of the highest electrical conductivities for oxides [4], while $SrRhO_3$ exhibits evidence of being affected by quantum critical fluctuations [5,6]. Other oxides of these elements are also of great interest, such as the superconducting Sr_2RuO_4 [7] and the pyrochlores $A_2Ru_2O_7$, which undergo metal to semiconductor transitions [8–10]. Technetium lies between molybdenum and ruthenium, but since all of its isotopes are radioactive, its solid state chemistry and physics have not been widely studied. Building on earlier work by Muller, White, and Roy [11], its metal oxides have recently come under scrutiny by modern physical methods [12–14]. In the present work we describe the synthesis of the perovskite $SrTcO_3$ and discuss its unusual magnetic and electronic properties.

Separate samples of $SrTcO_3$ were prepared by the groups in Australia and the U.S. The Sydney sample was obtained from a solid-state reaction between NH_4TcO_4 and $Sr(NO_3)_2$ at 700 °C for 1 h under argon and then ball milled in cyclohexane for 16 h, dried, pelleted, and then sintered under argon for 4 h at 1150 °C. The University of Nevada Las Vegas (UNLV) sample was prepared by a solid-state reaction between $SrCO_3$ and TcO_2 at 850 °C in a fused quartz boat under argon gas. Sample purity was confirmed by x-ray powder diffraction in each case.

Powder neutron diffraction data for the Sydney sample were collected on the high-resolution Echidna diffractometer at ANSTO's Opal facility at Lucas Heights using neutrons of wavelength 1.538 Å; data were obtained between room temperature and 750 °C in a standard vacuum furnace. The corresponding neutron data for the UNLV sample were collected on the NPDF diffractometer at the Manuel Lujan Neutron Scattering Center at LANL, where the data were collected in the time-of-flight mode between 4 and 500 K.

The room temperature constant wavelength (CW) data for $SrTcO_3$ were indexed on the basis of a perovskite cell in space group *Pnma* with $a \approx c \approx \sqrt{2}a_p$ and $b \approx 2a_p$ (where a_p is the lattice parameter of the cubic perovskite subcell) and refined by the Rietveld method [15] to yield the parameters given in Table I. The structure is that of the well-known $GdFeO_3$-type perovskite. The corresponding parameters for the time-of-flight refinement are given in parentheses [16]. Careful inspection of the Rietveld fit for the constant wavelength data reveals a peak at $\approx 19.4°$ 2θ that is not accounted for by the structural refinement [Fig. 1(a)]. The same peak is visible at a *d* spacing of 4.546 Å in the time-of-flight data, but was absent in the x-ray data (see supplemental material [17]).

The extra peak that is observed in both the constant wavelength and time-of-flight data can be indexed on the basis of the magnetic scattering expected from the *G*-type antiferromagnetic (AFM) structure with the moment directed along the *c* direction (Shubnikov group $Pn'ma'$)

TABLE I. Structural parameters for $SrTcO_3$ at 300 K. The lattice cell is orthorhombic with space group *Pnma* (62), and cell parameters are given below the table. Atomic displacement parameters are given in Å^2 and standard uncertainties are shown in parentheses. Structural and cell parameters from the time-of-flight results are shown in italics below those of CW data for comparison.

Atoms	Site	x	y	z	B_{iso}
Sr	4*c*	0.001(3)	1/4	0.507(3)	0.85(9)
		0.0086(5)	1/4	0.4995(5)	0.78(1)
Tc	4*a*	0	0	0	1.01(5)
		0	0	0	0.14(1)
O1	8*d*	0.262(2)	0.0327(5)	0.257(2)	0.76(14)
		0.2633(3)	0.0225(1)	0.2624(3)	0.82(2)
O2	4*c*	0.494(4)	1/4	0.524(5)	0.60(7)
		0.4961(8)	1/4	0.5416(3)	0.82(2)

$a = 5.5797(6)$ Å, $b = 7.8774(8)$ Å, $c = 5.5575(7)$ Å

$a = 5.5768(1)$ Å, $b = 7.8485(1)$ Å, $c = 5.5468(1)$ Å

shown in Fig. 2(a). Final refinement of the nuclear and magnetic structure yielded a magnetic moment of $1.87(4)\mu_B$ at room temperature, which increases to $2.13(4)\mu_B$ on cooling to 4 K. This is substantially lower than the spin-only value of $3.87\mu_B$ for a spin-only d^3 ion, probably due to covalency in the Tc–O bonds [18].

The possibility that the low-angle peak is due to some structural distortion of the oxygen atoms, and therefore missed by x rays, was considered. Since the (110) and (011) reflections are allowed for *Pnma* symmetry, the loss of the 19.4° 2θ peak at 750 °C could indicate a crystallographic transition at higher temperatures (as is common in perovskite oxides) rather than a magnetic one. This scenario, however, is irrefutably excluded by the fact that $SrTcO_3$ undergoes a crystallographic transition to the highest symmetry space group for a perovskite, $Pm\bar{3}m$, at 500 °C—well below the temperature at which the intensity of the peak is lost [Fig. 1(a)]. Thus, at temperatures above 500 °C, this reflection is already prohibited by symmetry and must be due to magnetic scattering from the Tc cations. Furthermore, the NPD pattern simulations show that nuclear contribution is negligible even for the *Pnma* symmetry [Fig. 1(b)]. Observation of only one magnetic reflection is no doubt a consequence of the sharp drop-off of the magnetic form factor for 4*d* and 5*d* electrons due to their highly delocalized nature; the second magnetic peak would appear at $\approx 38°$ 2θ, where the magnetic form factor has decreased strongly. Indeed, for ferromagnetic $SrRuO_3$ with a moment size of $\approx 1.6\mu_B$, the magnetic contribution to the NPD patterns is also minimal and confined to one peak at low 2θ [2,19].

The integrated intensity of the (110)/(011) reflections was used to follow the temperature evolution of the magnetic ordering. As can be seen from Fig. 1(c), $SrTcO_3$ shows very robust magnetic ordering up to 750 °C, which

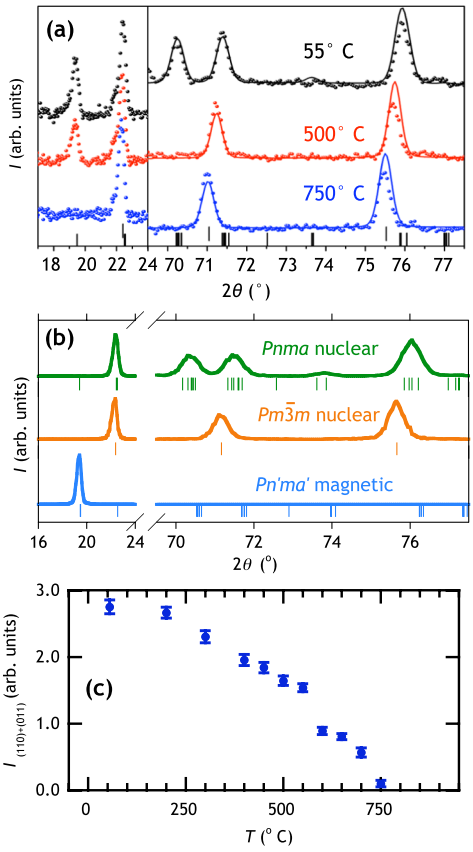

FIG. 1 (color online). (a) Observed constant wavelength NPD profiles of $SrTcO_3$; select 2θ regions are shown to highlight the change from *Pnma* symmetry to $Pm\bar{3}m$ symmetry and the loss of the magnetic peak at 19.4° 2θ upon heating. Tick marks for the cubic and orthorhombic structures are shown below the patterns, respectively. (b) Simulated contributions to the NPD patterns from the nuclear *Pnma* and $Pm\bar{3}m$ structures and the magnetic $Pn'ma'$ structure. (c) Temperature evolution of the magnetic peak from the CW data.

is entirely unprecedented for an oxide of the second transition metal series. Indeed, one of the unusual features of second row oxides is that magnetic ordering, if it occurs at all, is only observed at quite low temperatures. $SrRuO_3$, for

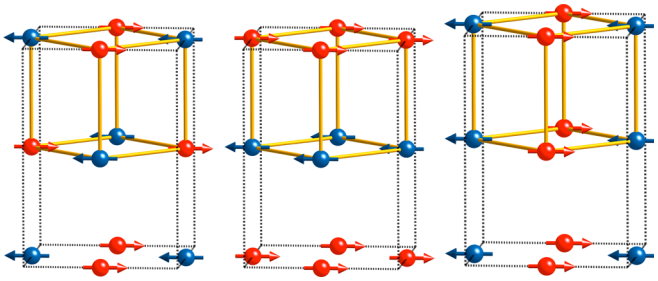

FIG. 2 (color online). (a) *G*-type antiferromagnetic ordering in the orthorhombic unit cell used for the structural refinement with the NPD data. (b) The *A*-type antiferromagnetic ordering and (c) *C*-type ordering. The sublattice with sides $\approx a_p$ [light gray (orange) line] corresponding to the cubic perovskite is drawn within the orthorhombic cells (thin dashed line).

example, has a Curie temperature of ≈ 160 K, whereas the analogous $SrCoO_3$ has a T_c of 280 K [20].

In order to shed further light on the magnetic ordering of $SrTcO_3$, we performed electronic structure calculations within the local density approximation using the general potential linearized augmented plane wave (LAPW) method including local orbitals [21]. These were done in a scalar relativistic approximation using the experimental orthorhombic crystal structure. Well-converged basis sets and other parameters were used, with LAPW sphere radii of 2.1 and 1.6 bohr for the metal and oxygen atoms, respectively.

The non-spin-polarized (NSP) density of states (DOS) is shown in Fig. 3(a). The NSP system is metallic, with a Fermi energy E_F in the middle of a manifold of nominal t_{2g} states, as expected from the electron count. However, unlike typical $3d$ oxides, these states are strongly hybridized with O. The Fermi energy is at the center of a prominent peak in the DOS, leading to a rather high $N(E_F) = 4.3$ eV^{-1} per Tc for both spins. This is a value that would substantially exceed the Stoner condition for a $3d$ based material leading to magnetism. However, the energy as a function of constrained ferromagnetic spin moment from fixed spin moment was calculated and resulted in no stable or metastable ferromagnetic state.

The nonexistence of ferromagnetic ordering can be inferred from the DOS. The projections show very strong covalency between O and Tc even for the nominal t_{2g} manifold (Tc t_{2g}-O p π-type antibonding combinations).

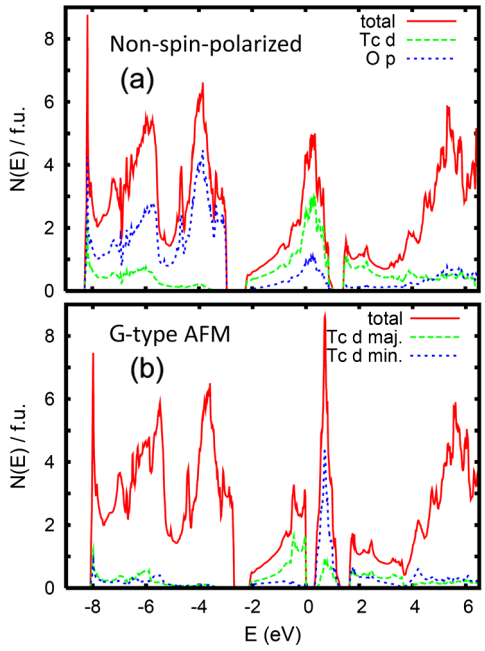

FIG. 3 (color online). (a) Electronic DOS and projections onto LAPW spheres for non-spin-polarized $SrTcO_3$. (b) Electronic DOS and majority and minority spin d projections onto the Tc LAPW sphere for G-type $SrTcO_3$.

Indeed, this is probably the cause for the reduced moment obtained from the neutron experiments. Because of this strong covalency, the Tc d character, as measured by the weight inside the 2.1 bohr LAPW sphere, amounts to only $\approx 60\%$ of the total $N(E_F)$. Furthermore the Hund's coupling on $4d$ atoms is smaller than that on $3d$ atoms because of the more extended orbitals. The combination of these two factors takes $SrTcO_3$ away from a Stoner instability even though $N(E_F)$ is high. In addition to the ferromagnetic fixed spin moment calculations, we also did calculations for other spin orders compatible with the primitive unit cell. These include the so-called A-type ordering, consisting of ferromagnetic sheets of Tc moments stacked antiferromagnetically along the [010] direction [Fig. 2(b)], the C-type arrangement with ferromagnetic sheets antialigned along the [100] and [001] directions [Fig. 2(c)], and finally the G-type nearest neighbor antiferromagnetic arrangement [Fig. 2(a)]. The A-type arrangement had no stable moments, while the C-type arrangement showed a very weak magnetic solution, with moments in the Tc LAPW spheres of $0.44\mu_B$ and an energy lower than the NSP state by only 0.4 meV/Tc. In contrast, a very robust solution was found for the G-type ordering. This has an energy 192 meV/Tc below the NSP with a Tc moment of $1.3\mu_B$. The G-type DOS [Fig. 3(b)] is strongly reconstructed by this ordering, and a small insulating band gap of 0.3 eV is opened.

In most oxide magnets there are two energy scales. The first is a scale set by intra-atomic Coulomb repulsions, particularly the Hund's coupling, which drive moment formation. This is typically a high energy scale and leads to stable moments at all solid-state temperatures. The second scale controls the ordering temperature, and is associated with the relative orientation of moments on neighboring sites. This is determined by interatomic hopping, as, for example, in the superexchange mechanism. In perovskites it arises from the hybridization between transition metal d orbitals and oxygen p orbitals [22,23]. Importantly, the ordering temperature is set by the energy differences between different configurations of the moments, and these differences in turn are related to metal oxygen covalency and details of the bonding topology. In $SrTcO_3$ the larger extent of the Tc $4d$ orbitals relative to, e.g., the $3d$ orbitals of Mn lowers the on-site interactions that underlie moment formation, but strongly increases the amount of covalency as seen in the DOS projections. The result is that the two energy scales become comparable and moment formation and ordering are intertwined. This type of situation is often described as itinerant magnetism. This term should, however, be used with caution, since the moments are not small, and as a result there is a rearrangement of the DOS not only near E_F but over most of the ≈ 3 eV wide t_{2g} manifold.

The G-type state can be understood in a simple chemical bonding type of picture. Hybridization occurs between states of the same global spin direction and gives the

strongest energy lowering when occupied states mix with unoccupied states. With *G*-type ordering, the occupied majority spin states on a given site hybridize with unoccupied minority states in the neighboring sites and vice versa. This is exactly the same mechanism that leads to *G*-type ordering in the analogous $3d\ t_{2g}^3$ materials, $CaMnO_3$ and $SrMnO_3$ [22,23].

There are two important differences between the perovskite manganites and $SrTcO_3$ that could result in a high ordering temperature in the latter. First, the energy scale is increased because of the greater hybridization and the smaller energy splitting between majority and minority spin orbitals (this enters in the denominator). Second, because the moment formation is intimately connected to the magnetic order, competing states, such as the *C*-type pattern, are suppressed. This is related to the physics that leads to high ordering temperatures in low moment itinerant magnets such as Cr and Ni metal. These two facts provide a qualitative explanation for the high Néel temperature of 750 °C in $SrTcO_3$. This result is in marked contrast to the behavior of $SrMoO_3$ and $SrRuO_3$, which are a highly conducting Pauli paramagnet and a metallic ferromagnet ($T_c \approx 160$ K), respectively. There is no significant structural difference between $SrMoO_3$, $SrRuO_3$, and $SrTcO_3$, since their bridging M–O–M angles are 170°, 163.6°, and 167.4°, respectively. Rather, the unique properties of $SrTcO_3$ stem from the high covalency of the Tc–O bonds combined with the outer $4d^3$ electron configuration of the Tc^{4+} cation.

This work has benefited from the use of NPDF and HIPD at the Lujan Center, funded by DOE Office of Basic Energy Sciences; LANL is operated by Los Alamos National Security LLC under DE-AC52-06NA25396. We would also like to thank the Australian Research Council for the work at the University of Sydney. Work at ORNL was supported by DOE, Basic Energy Sciences, Materials Sciences and Engineering Division.

[1] K. Isawa, J. Sugiyama, K. Matsuura, A. Nozaki, and H. Yamauchi, Phys. Rev. B **47**, 2849 (1993).
[2] J. M. Longo, P. M. Raccah, and J. B. Goodenough, J. Appl. Phys. **39**, 1327 (1968).
[3] I. I. Mazin and D. J. Singh, Phys. Rev. B **56**, 2556 (1997).
[4] I. Nagai, N. Shirakawa, S. Ikeda, R. Iwasaki, H. Nishimura, and M. Kosaka, Appl. Phys. Lett. **87**, 024105 (2005).
[5] K. Yamaura and E. Takayama-Muromachi, Phys. Rev. B **64**, 224424 (2001).
[6] D. J. Singh, Phys. Rev. B **67**, 054507 (2003).
[7] Y. Maeno, H. Hashimoto, K. Yoshida, S. Nishizaki, T. Fujita, J. G. Bednorz, and F. Lichtenberg, Nature (London) **372**, 532 (1994).
[8] W. Klein, R. K. Kremer, and M. Jansen, J. Mater. Chem. **17**, 1356 (2007).
[9] S. Lee *et al.*, Nature Mater. **5**, 471 (2006).
[10] J. van den Brink, Nature Mater. **5**, 427 (2006).
[11] O. Muller, W. B. White, and R. Roy, J. Inorg. Nucl. Chem. **26**, 2075 (1964).
[12] E. E. Rodriguez, F. Poineau, A. Llobet, A. P. Sattelberger, J. Bhattacharjee, U. V. Waghmare, T. Hartmann, and A. K. Cheetham, J. Am. Chem. Soc. **129**, 10 244 (2007).
[13] E. E. Rodriguez, F. Poineau, A. Llobet, K. Czerwinski, R. Seshadri, and A. K. Cheetham, Inorg. Chem. **47**, 6281 (2008).
[14] E. E. Rodriguez, F. Poineau, A. Llobet, J. D. Thompson, R. Seshadri, and A. K. Cheetham, J. Mater. Chem. **21**, 1496 (2011).
[15] J. Rodríguez-Carvajal, Physica (Amsterdam) **192B**, 55 (1993).
[16] A. C. Larson and R. B. Von Dreele, Los Alamos National Laboratory, Technical Report No. LAUR 86-748, 2004.
[17] See supplemental material at http://link.aps.org/supplemental/10.1103/PhysRevLett.106.067201 for time-of-flight and constant wavelength neutron powder patterns of $SrTcO_3$ and an x-ray powder pattern.
[18] J. Hubbard and W. Marshall, Proc. Phys. Soc. London **86**, 561 (1965).
[19] S. N. Bushmeleva, V. Y. Pomjakushin, E. V. Pomjakushina, D. V. Sheptyakov, and A. M. Balagurov, J. Magn. Magn. Mater. **305**, 491 (2006).
[20] P. Bezdicka, A. Wattiaux, J. C. Grenier, M. Pouchard, and P. Hagenmuller, Z. Anorg. Allg. Chem. **619**, 7 (1993).
[21] D. J. Singh and L. Nordstrom, *Planewaves, Pseudopotentials and the LAPW Method* (Springer-Verlag, Berlin, 2006), 2nd ed.
[22] J. B. Goodenough, *Magnetism and the Chemical Bond* (John Wiley & Sons, New York, 1963).
[23] P. W. Anderson, Phys. Rev. **115**, 2 (1959).